Development of a Lumped Element Circuit Model for Approximation of Nanosecond Pulsed Dielectric Barrier Discharges

Thomas C. Underwood* and Subrata Roy†

Computational Plasma Dynamics Laboratory and Test Facility,
Applied Physics Research Group, Mechanical and Aerospace Engineering,
University of Florida, Gainesville, FL 32611

Bryan Glaz‡

Vehicle Technology Directorate, U.S. Army Research Laboratory, MD 21005

This work presents a circuit model for calculating the total energy dissipated into neutral species for nanosecond pulsed direct current (DC) dielectric barrier discharge (DBD) plasmas. Based on experimental observations, it is assumed that the nanosecond pulsed DBD's which have been proposed for aerodynamic flow control can be approximated by two independent regions of homogeneous electric field. An equivalent circuit model is developed for both homogeneous regions based on a combination of a resistor, capacitors, and a zener diode. Instead of fitting the resistance to an experimental data set, a formula is established for approximating the resistance by modeling plasmas as a conductor with DC voltage applied to it. Various assumptions are then applied to the governing Boltzmann equation to approximate electrical conductivity values for weakly ionized plasmas. The developed model is then validated with experimental data of the total power dissipated by plasmas.

Nomenclature

$\mathbf{B}$	Magnetic Field, T
C	Capacitance, F
$\mathbf{E}$	Electric Field, V/m
$\mathbf{J}$	Current Density, A/m^2
l	Chordwise Length, m
m	Mass, kg
N_a	Number Density of Atoms, m^{-3}
N_e	Number Density of Electrons, m^{-3}
P	Power, W
Q	Energy, J
R	Resistance, Ω
$\mathbf{v}$	Velocity, m/s
V	Voltage, V
V_{app}	Applied Voltage, V
V_{vol}	Volume, m^3
w_e	Drift Velocity of Electrons, m/s
Γ_e	Electron Flux, m^{-2}s^{-1}
ϵ_a	Relative Dielectric Constant of Air

*Undergraduate Student, University of Florida
†Associate Professor, AIAA Associate Fellow
‡Research Aerospace Engineer, AIAA Senior Member

Report Documentation Page

Form Approved
OMB No. 0704-0188

1. REPORT DATE	2. REPORT TYPE	3. DATES COVERED
2013		**00-00-2013 to 00-00-2013**

4. TITLE AND SUBTITLE	5a. CONTRACT NUMBER
Development of a Lumped Element Circuit Model for Approximation of Nanosecond Pulsed Dielectric Barrier Discharges	5b. GRANT NUMBER
	5c. PROGRAM ELEMENT NUMBER
6. AUTHOR(S)	5d. PROJECT NUMBER
	5e. TASK NUMBER
	5f. WORK UNIT NUMBER
7. PERFORMING ORGANIZATION NAME(S) AND ADDRESS(ES) **University of Florida,Applied Physics Research Group,Department of Mechanical and Aerospace Engineering,Gainesville,FL,32611**	8. PERFORMING ORGANIZATION REPORT NUMBER
9. SPONSORING/MONITORING AGENCY NAME(S) AND ADDRESS(ES)	10. SPONSOR/MONITOR'S ACRONYM(S)
	11. SPONSOR/MONITOR'S REPORT NUMBER(S)

12. DISTRIBUTION/AVAILABILITY STATEMENT
Approved for public release; distribution unlimited

13. SUPPLEMENTARY NOTES
51st AIAA Aerospace Sciences Meeting, 7-10 Jan 2013, Grapevine, TX. U.S. Government or Federal Rights License

14. ABSTRACT

15. SUBJECT TERMS

16. SECURITY CLASSIFICATION OF:			17. LIMITATION OF ABSTRACT	18. NUMBER OF PAGES	19a. NAME OF RESPONSIBLE PERSON
a. REPORT	b. ABSTRACT	c. THIS PAGE			
unclassified	**unclassified**	**unclassified**	**Same as Report (SAR)**	**18**	

ϵ_d Relative Dielectric Constant of Material
λ_D Debye Length, m
ν Collision Frequency, s^{-1}
σ Scattering Cross Section, m^2
σ_p Conductivity of Plasma, S/m
σ_s Conductivity of Sheath, S/m
τ Relaxation Time, s

I. Introduction

The need for improved control over aerodynamic flow separation has increased interest in the potential use of plasma actuators. The inherent advantages of plasma actuator flow control devices include: fast response time, surface compliance, lack of moving parts, and inexpensiveness. However, it has been established that the actuators which affect the flow via directed momentum transfer are not effective at Mach numbers associated with most subsonic aircraft applications. Recently, Roupassov et. al[10] demonstrated that pulsed plasma actuators, in which energy imparted to the flow appears to effectively control flow separation, seem to be suitable at Mach numbers (M≈0.3) beyond the capabilities of the current plasma induced momentum based approaches.

Given the fundamental differences between the novel pulsed discharge approach and the more conventional momentum based approaches, there is a need to develop an effective and efficient model for the energy delivered to the flow by the plasma. Once calculated, that value can be input to a computational fluid dynamics solver as an energy source term resulting in a coupled fluid/plasma dynamics model. Multiphysics models of this type are required in order to study detailed flow characteristics. However, detailed numerical simulations involving plasma kinetics are computationally prohibitive for a variety of coupled fluid/plasma design problems. To address this issue, efficient circuit element models have been introduced to approximate the complex processes within plasmas. Circuit models such as those by Orlov et. al[6] rely on empirical constants which may not be applicable to nanosecond pulsed discharges. To date, an approximate model of nanosecond pulsed plasma actuators has not been developed. This paper deals primarily with establishing a flexible model with relevant physics that could be implemented as an approximation for the energy dissipated within a plasma for any pulsed DC DBD configuration. Among the other goals in this paper is to probe into the background processes that occur within plasmas and incorporate that knowledge into the model.

II. Lumped Element Circuit Model

One of the primary assumptions in creating this model is that nanosecond pulsed DBD's can be approximated by two independent regions of homogeneous electric field. One such region, dubbed the 'hot spot' is the region adjacent to the powered electrode. This region makes up a small portion of the total discharge area but was observed to be an important component of the plasma discharge and necessary to obtain agreement with experimentally measured shock wave dynamics by Roupassov et. al.[10] The other region, dubbed the 'tail,' encompasses the rest of the plasma discharge and extends to the edge of the dielectric. As both regions are independent, the model presented in this paper consists of a single network for each region containing a resistor, capacitors, and a diode.

As shown in Fig. 1, circuit elements that were used to model the plasma include: an air capacitor C_a, a dielectric capacitor C_d, a resistor R_f, and a zener diode D_f. The air capacitor represents the capacitance between the dielectric surface and the exposed electrode. The dielectric capacitor represents the capacitance between the dielectric surface and insulated electrode and is proportional to the thickness of the dielectric layer. Thus the dielectric layer in the form of both its thickness and the value of its dielectric constant plays an important role in determining the effectiveness of the plasma actuator. Finally, the zener diode, introduced by Orlov et. al,[6] is utilized in the model to enforce an energy threshold value below which plasma will not form.

Since a uniform charge distribution along the top of the dielectric is assumed, the typical asymmetric 2-D

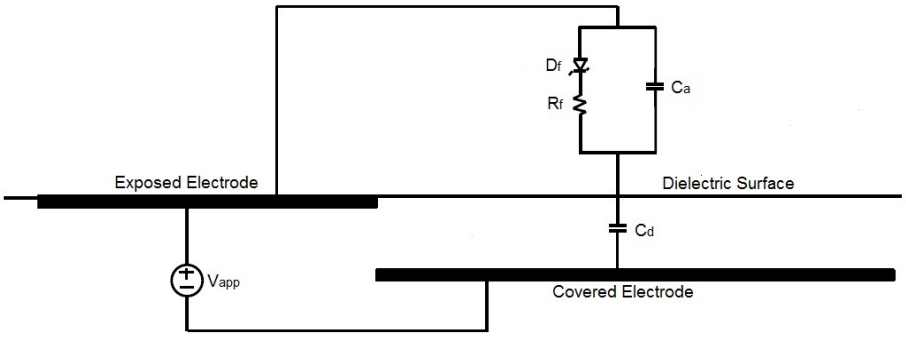

Figure 1. Electric circuit model of a dielectric aerodynamic plasma actuator.

plasma actuator geometry featured in Fig. 1 can be simplified to a series of homogeneous symmetric regions. As shown in Fig. 2, these regions include: an anode sheath, 'hot spot', and 'tail.'

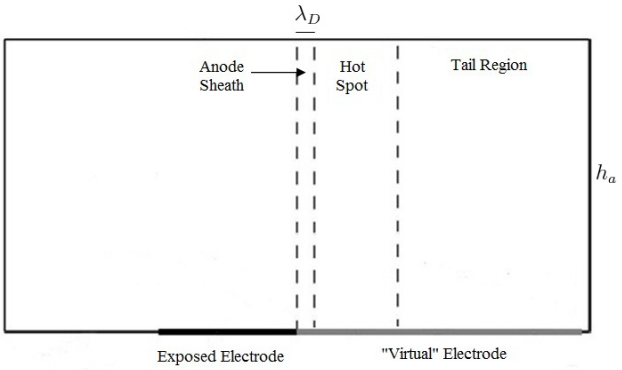

Figure 2. Plasma discharge regions.

This assumption results in a series of coupled 1-D models that account for the chordwise variation along the actuator. Fig. 3 shows the simplified circuit model within each homogeneous region.

A. Circuit

As displayed in Fig. 1, the lumped element circuit is a function of the two capacitance values, C_a and C_d. In this model, the air is treated as both a conductor to generate a physical relationship for the resistance R_f and a parallel plate capacitor to generate C_a. An advantage of modeling the plasma as a conductor in addition to a parallel plate capacitor is that it generates a physical relationship for the resistance, R_f, a value that is traditionally empirically determined. The air gap capacitor can be modeled as[4]

$$C_a = \frac{\epsilon_0 \epsilon_a A_a}{h_a}, \tag{1}$$

where A_a is the cross-sectional area of the air and h_a is the approximate height of the plasma region of interest. The height of the plasma has been shown by Roupassov et. al[10] to be approximately independent of applied voltage for nanosecond pulsed DBD actuators. As displayed in Fig. 4, A_a is the product of the spanwise length of the actuator z_a, and l_a is the chordwise distance from the exposed electrode to the end of the dielectric region.

The capacitive element corresponding to the dielectric can be modeled as[4]

$$C_d = \frac{\epsilon_0 \epsilon_d A_d}{h_d}, \tag{2}$$

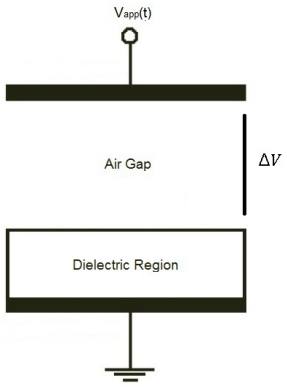

Figure 3. Region of homogeneous potential.

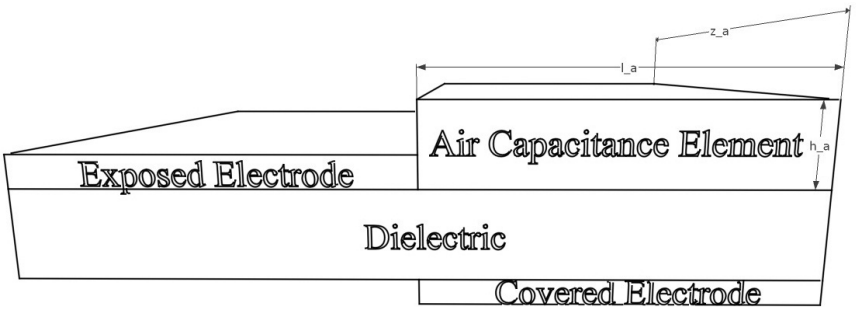

Figure 4. Sketch of the capacitive air element.

where A_d is the cross-sectional area of the dielectric capacitive element and h_d is the height of the dielectric barrier layer. As displayed in Fig. 5, A_d is the product of the spanwise length of the actuator z_a and d_d, the width of the dielectric region. Treating the plasma as a conductor, the resistance for DC voltage is proportional to σ_p, A_a, and h_a and can be given as[4]

$$R_f = \frac{h_a}{\sigma_p A_a}. \tag{3}$$

Starting from Kirchoff's circuit laws,[4] the governing differential equation for the voltage drop experienced by the air gap, ΔV, is given by

$$\frac{d\Delta V(t)}{dt} = -\frac{dV_{app}}{dt}\left(\frac{C_a}{C_a + C_d} - 1\right) - \kappa \frac{\Delta V(t)}{R_f(t)\,(C_a + C_d)}, \tag{4}$$

$$\kappa = \begin{cases} 1 & \text{if } |\mathbf{E}| > E_{crit}, \\ 0 & \text{if } |\mathbf{E}| \leq E_{crit}. \end{cases} \tag{5}$$

where V_{app} is the applied voltage and κ is the contribution from the zener diode. If the electric field magnitude, given as

$$|\mathbf{E}| = \frac{|\Delta V|}{h_a}, \tag{6}$$

is greater than the breakdown electric field,[6] E_{crit}, required to ionize air, then κ takes on a value of one, otherwise it is zero to signify that plasma has not formed.

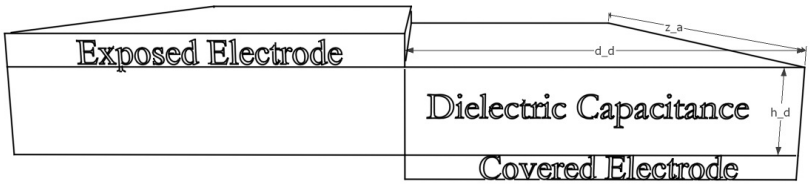

Figure 5. Sketch of the dielectric capacitive element.

B. Conductivity

To effectively calculate the resistance governed by Eq. 3, an expression must first be developed for the electrical conductivity, σ_p, of the plasma. This value is one that traditionally requires a numerical approach. To simplify the problem to a point where an analytic formulation can be used, numerous simplifying assumptions were used and are described in the following paragraphs.

For any plasma, the resulting electric current is composed of two primary terms: the current from electrons and that from ions. As the drift velocity of electrons, $\mathbf{w}_e$, in a non-equilibrium plasma is significantly higher than ions, the current density can be approximated as the portion from electrons if the number densities, N_e and N_i, are approximately the same. Using a form of the generalized Ohm's Law, the current density vector, $\mathbf{J}$ and σ_p respectively can be written as

$$\mathbf{J} \approx -eN_e\mathbf{w_e} = \sigma_p\mathbf{E}, \tag{7}$$

$$\sigma_p = e\left(N_e\mu_e + N_i\mu_i\right), \tag{8}$$

where μ_i and μ_e represent the ion and electron mobilities respectively. Much like Eq. 7, the electrical conductivity relation can be simplified using the concept of quasineutrality which is defined as having approximate equal number densities for charged particles of opposite polarity. Thus as μ_e is typically three orders of magnitude larger than μ_i, it is a good assumption to approximate the electrical conductivity as only coming from electrons as long as N_e is at least of the same order of magnitude as N_i.[7] Quasineutrality is a typical assumption that is valid as long as the plasma being modeling is far enough away from the powered electrode to avoid the boundary layer in plasma physics called the sheath.

Since a pulsed DC voltage is assumed, the activation of the external electric field will follow the voltage waveform as a step function. Thus two expressions will be required for σ_p, where the first is valid for the period when an external electric field is applied, as shown in Fig. 9 from 0-65 ns, and the second when the voltage drop over the air gap is zero. For the portions of the voltage waveform that ΔV is zero, the power is also zero according to Ohm's Law and thus the conductivity during this time is of no importance.

To generate a analytic formula for the electrical conductivity, a distribution function must be introduced to describe the physical evolution in the number of particles, $f(\mathbf{v}, J, \mathbf{r}, t)$, defined such that $f(\mathbf{v}, J, \mathbf{r}, t)\ d\mathbf{v}$ is the number of particles in a unit volume located at point $\mathbf{r}$, time t, internal quantum number J, and differential velocity range $\mathbf{v} + d\mathbf{v}$. Using this distribution function, the number of particles at point $\mathbf{r}$ and time t can be defined as

$$N(\mathbf{r}, t) = \sum_J \int f(\mathbf{v}, J, \mathbf{r}, t) d\mathbf{v}. \tag{9}$$

This distribution function allows a mathematical description to be developed for the temporal evolution in the number of particles resulting from particle collisions within a control volume. The time rate of change in the number of particles due to externally applied fields can be described as[11]

$$\frac{Df}{Dt} = \frac{f(\mathbf{v} + d\mathbf{v}, J, \mathbf{r} + d\mathbf{r}, t + dt) - f(\mathbf{v}, J, \mathbf{r}, t)}{dt}. \tag{10}$$

A partial differential equation can be developed to describe Eq. 10 using formulas for the time rate of change of $\mathbf{v}$ and $\mathbf{r}$ established by using the equation of motion in the form of

$$\frac{d\mathbf{v}}{dt} = \frac{\mathbf{F}}{m}, \tag{11}$$

$$\frac{d\mathbf{r}}{dt} = \mathbf{v}, \tag{12}$$

and the chain rule of calculus to obtain the Boltzmann kinetic energy equation given as

$$\frac{Df}{Dt} = \frac{\partial f}{\partial t} + \mathbf{v} \cdot \frac{\partial f}{\partial \mathbf{r}} + \frac{\mathbf{F}}{m} \cdot \frac{\partial f}{\partial \mathbf{v}}. \tag{13}$$

In order to approximate the total derivative, a relaxation time can be introduced defined as the time taken for the system to be reduced to an equilibrium distribution function. The tau approximation can be given as $\tau \approx (N_a \sigma_{ea} |\mathbf{v}|)^{-1}$ where σ_{ea} is the collision cross section between electrons and atoms, $|\mathbf{v}|$ is the average collision velocity, and N_a is the number density of atoms.[11] If the number of particles within a control volume is defined as a equilibrium distribution function, f_0, when each particle is at the same energy level as its neighbor, then the particle evolution over time due to pairwise collisions after an external force has been applied can be given as[11]

$$\frac{Df}{Dt} = -\frac{f - f_0}{\tau}. \tag{14}$$

As τ only accounts for collisions between electrons and neutral atoms, it is only accurate in the event of a weakly ionized plasma. Plasma actuators considered in this paper traditionally feature a low degree of ionization, or simply the amount of air that is ionized, and thus can be treated in a weakly ionized limit. In terms of the momentum-transfer collision frequency which can be defined as the mass corrected rate at which a particle of a specific species collides with another, the criteria for a weakly ionized plasma can be given as[7]

$$\bar{\nu}_{ei} << \bar{\nu}_{en}. \tag{15}$$

This equation requires that the collision frequency between electrons and ions be much less that those between electrons and neutrals. Thus, if this requirement is met, the collisional occurrences between electrons and charged particles can be effectively ignored and the relaxation time established is a good approximation of the total time rate of change in the number of particles within a control volume.

After introducing a relaxation time to approximate Eq. 13, an equation of motion describing the average velocity of electrons can be established by multiplying by $m_e \mathbf{v}$ and integrating over the electron velocity. An analytic formulation for the average velocity an electron experiences due to an externally applied field, $\mathbf{w}_e$, can be obtained by assuming that the force term can be approximated as the Lorentz force,

$$\mathbf{F} = -e\mathbf{E} - \frac{e}{c}\left(\mathbf{v} \times \mathbf{B}\right), \tag{16}$$

where $\mathbf{B}$ represents the magnetic field and $\mathbf{E}$ represents the electric field. As plasma actuators have no applied magnetic field, $\mathbf{B}$ can be set equal to zero. Therefore the equation of motion for an electron describing $\mathbf{w}_e$ can be given as

$$m_e \frac{d\mathbf{w_e}(t)}{dt} + m_e \frac{\mathbf{w_e}(t)}{\tau} = -e\mathbf{E}(t). \tag{17}$$

Solving Eq. 17, a linear first-order differential equation, an integral equation is obtained:

$$w_e(t^*) = -\frac{e}{m_e} \exp\left(-\frac{t^*}{\tau^*}\right) \int_0^{t^*} E(t) \exp\left(\frac{t}{\tau^*}\right) dt. \tag{18}$$

Eq. 18 can be solved in conjunction with Eq. 7 to obtain an expression for the time varying conductivity and in conjunction with Eq. 8 to obtain an approximation for the time varying electron mobility if the ion mobility is neglected. The electrical conductivity and electron mobility respectively can be given as

$$\sigma_p(t^*) = \frac{N_e(t^*)e^2}{m_e E(t^*)} \int_0^{t^*} E(t) \exp\left(\frac{t - t^*}{N_a^* \sigma_{ea}^* \nu^*}\right) dt, \tag{19}$$

$$\mu_e(t^*) \approx \frac{e}{m_e E(t^*)} \int_0^{t^*} E(t) \exp\left(\frac{t - t^*}{N_a^* \sigma_{ea}^* \nu^*}\right) dt, \tag{20}$$

where σ_{ea} is a function of electron energy and can be obtained for various molecules found in air from Phelps.[8] Numerical values used in the model are included in the Appendix. The electron velocity can be obtained by assuming a Maxwellian velocity profile. As a collection of electrons within plasma have a range of velocities, the Maxwellian velocity profile represents the most probable distribution of these velocities. Thus the distribution of velocities, $f(u,v,w)$, can be given by[7]

$$f(u,v,w) = A_3 \exp\left[-\frac{\frac{1}{2}m\left(u^2+v^2+w^2\right)}{k_b T_e}\right], \tag{21}$$

$$A_3 = N_e\left(\frac{m}{2\pi k_b T_e}\right)^{\frac{1}{2}}. \tag{22}$$

Using the non-relativistic definition of kinetic energy, a relationship can be established for the kinetic energy of an electron that is valid in the limit $|\mathbf{v}| << c$, where c is the speed of light. Using this approximation, the relativistic formulation of the kinetic energy can be approximated as

$$E_k = \frac{mc^2}{\sqrt{1-|\mathbf{v}^2|/c^2}} - mc^2 \approx \frac{1}{2}m\mathbf{v}^2. \tag{23}$$

Averaging Eq. 21 and using the non-relativistic definition of kinetic energy, the mean kinetic energy of electrons becomes[7]

$$E_{av} = \frac{\iiint_{-\infty}^{\infty} A_3 \frac{1}{2}m_e\left(u^2+v^2+w^2\right)\exp\left[-\frac{1}{2}m_e\left(u^2+v^2+w^2\right)/k_b T_e\right]\,du\,dv\,dw}{\iiint_{-\infty}^{\infty} A_3 \exp\left[-\frac{1}{2}m_e\left(u^2+v^2+w^2\right)/k_b T_e\right]\,du\,dv\,dw} = \frac{3}{2}k_b T_e, \tag{24}$$

where k_b is Boltzmann's constant. From the definition of kinetic energy, the relationship between E_{av} and $|\mathbf{v}|$ with vector components (u,v,w) can be established and the average thermal velocity of electrons becomes

$$|\mathbf{v}| = \sqrt{\frac{3k_b T_e}{m_e}}. \tag{25}$$

The required inputs for Eqs. 19-20 include: N_e the number density of electrons, N_a the number density of atoms, and T_e the temperature of the electrons. Among these values, N_a can be assumed to be constant in time as the number density of atoms is significantly higher than that of free electrons.

Many other models incorporate a constant electron temperature into their model.[5,6] Using experimentally measured values of reduced electric field strength,[1] E/N_a vs. electron temperature as detailed in Fig. 6, this model calculates a new electron temperature at each time step by comparing the E/N value experienced by the plasma, produced from using Eqs. 4-6, with Fig. 6. It is assumed in this paper that the effects of an applied electric field have an instantaneous, or on a time scale much faster than 10^{-9} s, effect on electrons.

A time-varying differential equation that governs N_e can be obtained from the drift-diffusion equations. The electron continuity equation that governs N_e can be given by

$$\frac{\partial N_e}{\partial t} + \nabla\cdot\mathbf{\Gamma_e} = \alpha|\mathbf{\Gamma}_e| - \beta n_i n_e, \tag{26}$$

where $\mathbf{\Gamma}_e$ is called the charged species flux, α is the Townsend coefficient of ionization, and β is the recombination coefficient between electron and neutral atoms. By simplifying the plasma discharge into a combination of two homogeneous regions plus an anode sheath and by invoking the irrotational property of electric fields, Eq. 26 can be simplified by ignoring any spatial variation in the number density of electrons i.e. $\mathbf{\Gamma}_e$ becomes

$$\mathbf{\Gamma_e} \approx N_e\mu_e|\mathbf{E}|. \tag{27}$$

Assuming the number densities of electrons and ions are equal i.e. in the quasineutral region, the electron continuity equation for air, with a composition of 80% N_2 and 20% O_2, can be written as

$$\frac{dN_e}{dt} \approx \alpha_{air}|N_e\mu_e\mathbf{E}| - 0.80\beta_{N2}N_e^2 - 0.20\beta_{O2}N_e^2, \tag{28}$$

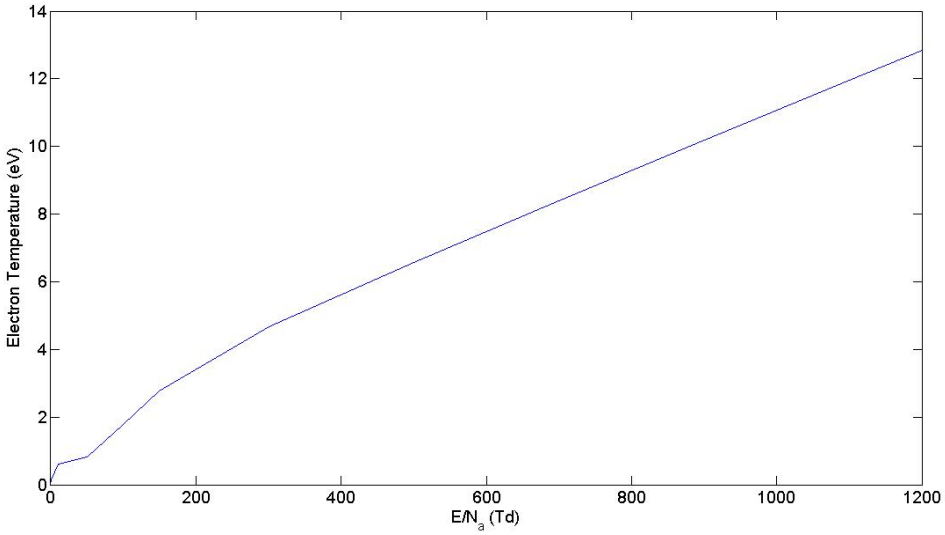

Figure 6. Plot of electron temperature vs. reduced electric field.

where α_{air} and β respectively can be approximated as having the form[9]

$$\alpha_{air} = Ap \exp\left(-\frac{Bp}{E}\right), \tag{29}$$

$$\beta_{N2} = 2.8 \times 10^{-7} \left(\frac{300}{T_e}\right) [\mathrm{cm}^3/\mathrm{s}], \tag{30}$$

$$\beta_{O2} = 2 \times 10^{-7} \left(\frac{300}{T_e}\right) [\mathrm{cm}^3/\mathrm{s}], \tag{31}$$

where A and B are empirical constants that have tabulated values of 15 and 365 respectively for air at atmospheric pressure.[9]

C. Discharge Development

The final remaining unknown required to close the equation system is to determine how the electric potential changes over the horizontal length of the actuator. To accurately model this, it is important to incorporate the wall effects of the plasma actuator. In terms of potential variation, these wall effects attract charged particles of opposite polarity and shield charged particles of the same polarity. Therefore for regions beside the anode (powered electrode for positive pulses), an anode sheath is developed where an attraction of electrons occurs and a repulsion of positive ions occur. For regions above the dielectric region on top of the grounded electrode, a cathode sheath is developed where positive ions are collected and electrons are repelled. Fig. 7 illustrates the two predominate sheaths that are developed in asymmetric plasma actuators.

It is important to consider the effects of charge collection and repulsion in these regions as such phenomenon can have large effects on the variation of the electric potential over the chordwise length and height of the plasma discharge.

Wall Effects

As this model is interested in solving the amount of energy the plasma transfers to neutral species, the relative importance of both the anode and cathode sheath regions needs to be established. Energy, Q, is a function of electrical conductivity and electric field strength and can be given as[7]

$$Q = \sigma_p |\mathbf{E}^2| V_{vol}. \tag{32}$$

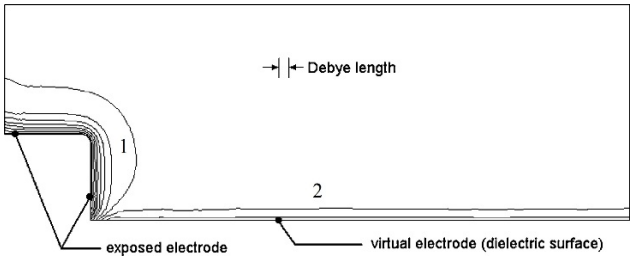

Figure 7. Collective wall effects of the exposed powered electrode and virtual electrode (dielectric region). 1- Anode Sheath, 2- Cathode Sheath.[3]

Eq. 32 shows that the energy transfer from both sheath regions is proportional to the conductivity of the plasma within each region. As the cathode sheath region typically has very few electrons due to repulsion effects, the current within this region will be carried by positively charged ions. The mobility of such ions are significantly less than that of an electron, so as a first order approximation if the local charged species number density and electric field strength are assumed equal, the conductivity in the cathode sheath will be significantly less than the conductivity in a bulk plasma and the anode sheath i.e.

$$\sigma_{s-c} << \sigma_p \approx \sigma_{s-a}. \tag{33}$$

When combined with the fact that the volume of both sheath regions are orders of magnitude less than the bulk plasma, an order of magnitude approximation to the plasma discharge can be obtained by ignoring the cathode sheath's effects for nanosecond pulsed plasma discharges. Although the cathode sheath is approximately negligible in terms of energy transfer, the higher electric field strength and higher conductivity present in the anode sheath contains important physics necessary for capturing the energy transferred by a plasma discharge.

Fig. 2 shows the updated 'hot spot' and 'tail' regions with the anode sheath included in the hot spot region adjacent to the powered electrode.

Electric Potential Variation

To establish a variation in the electric potential, the governing Maxwell equations can be used which are written as[4]

$$\nabla \cdot \mathbf{E} = \frac{\rho_f}{\epsilon_0}, \tag{34}$$

$$\nabla \cdot \mathbf{B} = 0, \tag{35}$$

$$\nabla \times \mathbf{E} = -\frac{\partial B}{\partial t}, \tag{36}$$

$$\nabla \times \mathbf{B} = \mu_0 \mathbf{J} + \mu_0 \epsilon_0 \frac{\partial E}{\partial t}, \tag{37}$$

in differential form where $\rho_f = e\,(n_i - n_e)$ is the net charge density and μ_0 is the permeability of free space. In the absence of a time-varying magnetic field, Eq. 36, Faraday's Law of Induction, simplifies to

$$\nabla \times \mathbf{E} = 0, \tag{38}$$

and since the curl of $\mathbf{E}$ is zero, the electric field can be solved for as a potential function ϕ and substituted into Gauss' Law, Eq. 34. The resulting equations respectively can be given by

$$\mathbf{E} = -\nabla\phi, \tag{39}$$

$$\nabla^2\phi = -\frac{\rho_f}{\epsilon}. \tag{40}$$

The net charge density within the quasineutral region of a plasma is equal to zero as $n_e = n_i$. For the anode sheath, the net charge density can be approximated if the plasma is assumed to uniformly distribute its

charge density. Therefore the quasineutral region of the 'hot spot' and 'tail' feature equal number densities of both electrons and ions ($n_e = n_i$) while the cathode and anode sheaths only have electron and ion densities respectively. If this is assumed then the anode sheath can be approximated as having a net charge density equal to the quasineutral region's calculated electron number density. By assuming the anode sheath is devoid of any positive ions and has a time-dependent number density of electrons, Poisson's equation for the sheath can be given by

$$\frac{d^2\phi}{dx^2} = \frac{eN_e(t)}{\epsilon_0}. \tag{41}$$

If this form is assumed for a single Debye length (λ_D), then the remaining discharge (rest of 'hot spot' and 'tail') region is part of the quasineutral bulk plasma and can be given by Laplace's equation

$$\frac{d^2\phi}{dx^2} = 0. \tag{42}$$

The ordinary differential equations for electric potential variation in the hot spot and tail regions respectively can be solved to provide an approximate 1-D spatial variation.

$$\phi(x) = \begin{cases} \frac{eN_e}{2\epsilon_0}x^2 + C_1x + C_2 & \text{if } x \leq \lambda_D \\ C_3x + C_4 & \text{if } x > \lambda_D \end{cases} \tag{43}$$

Eq. 43 requires a total of 4 boundary conditions. Those can be summarized as

$$\phi_1(x = 0) = V_{app}, \tag{44}$$
$$\phi_2(x = L) = V_{break}, \tag{45}$$
$$\phi_1(x = \lambda_D) = \phi_2(x = \lambda_D), \tag{46}$$
$$\frac{d\phi_1}{dx}(x = \lambda_D) = \frac{d\phi_2}{dx}(x = \lambda_D), \tag{47}$$

where ϕ_1 is the potential in the anode sheath, ϕ_2 is the potential in the quasineutral region, L is length of the actuator and λ_D is a Debye length. The first boundary condition is V_{app} at the cathode and the second is based on experimental observations by Roupassov et. al.[10] It was observed that a plasma discharge could be approximated as stopping at the edge of the grounded electrode for asymmetric actuators independent of the applied voltage; so the edge represents the absolute limit of ionization or the breakdown voltage of air. Using Eqs. 44-47 as boundary conditions, the potential becomes Eq. 48.

$$\phi(x) = \begin{cases} \frac{eN_e}{2\epsilon_0}x^2 + \left[\frac{eN_e}{2\epsilon_0 L}x_0^2 - \frac{eN_e}{\epsilon_0}x_0 + \frac{V_{break}-V_{app}}{L}\right]x + V_{app} & \text{if } x \leq \lambda_D \\ \left[\frac{eN_e}{2\epsilon_0 L}x_0^2 - \frac{eN_e}{\epsilon_0}x_0 + \frac{V_{break}-V_{app}}{L}\right](x - L) + V_{break} & \text{if } x > \lambda_D \end{cases} \tag{48}$$

The Debye length provides an order of magnitude approximation for the extent of a plasma sheath by assuming an exponential Boltzmann distribution in the charge density within the plasma discharge. Substituting this into Poisson's Eq.,

$$\epsilon_0\frac{d^2\phi}{dx^2} = eN_\infty\left[\exp\left(\frac{e\phi}{k_bT_e}\right) - 1\right], \tag{49}$$

where N_∞ is the charged particle density far away from the electrode. Taking a first-order Taylor expansion, the Debye length can be given as[7]

$$\lambda_D \sim \left(\frac{\epsilon_0 k_b T_e}{N_\infty e^2}\right)^{\frac{1}{2}}. \tag{50}$$

Although at high voltages, a first-order approximation fails, Eq. 50 still provides an order of magnitude approximation of the extent of the anode sheath.

D. Numerical Procedure

When solving for the energy imparted to neutral species, a coupled equation system results from Eqs. 4 and 28. The coupled terms include:

$$R_f \propto N_e, \tag{51}$$
$$\Gamma_e \propto \Delta V, \tag{52}$$
$$\beta \propto \Delta V, \tag{53}$$
$$\phi_1 \propto N_e. \tag{54}$$

To solve the resulting equation system, the Dormand-Prince Runge-Kutta method was employed. This method provides an efficient way to incorporate an adaptive step size that is important for computational efficiency in a problem that requires small time steps for convergence. The benefit of such a procedure can be illustrated through a simplistic example. If the error of each time step is defined as

$$\epsilon_k^i = y(t) - y_k^i, \tag{55}$$

then if two step sizes are considered, h_1 and h_2, the error of each iteration and their relative error respectively can be given as

$$y(t) - y_{n1}^{(1)} = \epsilon_{n1}^{(1)} = ah_1, \tag{56}$$
$$y(t) - y_{n2}^{(2)} = \epsilon_{n2}^{(2)} = ah_2, \tag{57}$$
$$y_{n2}^{(2)} - y_{n1}^{(1)} = a(h_1 - h2). \tag{58}$$

Therefore for a given error tolerance, ϵ, a sequence of step sizes can be generated,

$$h_{i+2} = q\frac{(h_i - h_{i+1})\,\epsilon}{|y_{n_{i+1}}^{(i+1)} - y_{n_i}^{(i)}|}, \tag{59}$$

which allows a numerical ODE solver, such as those employing the Dormand-Prince method to minimize functional error by adjusting the step size after each time step.[2] Numerical integration required for Eqs. 19-20 and energy derived from the circuit model, given as

$$Q = \int_0^t \frac{\Delta V^2}{R_f(t)} dt, \tag{60}$$

were performed via the Gauss-Kronrod quadrature method[2] at each time step.

III. Results

A. Validation Against Experiment

To validate the accuracy of the model described in this paper, comparisons with data presented in Roupassov et. al[10] is provided. The experimental parameters that were mentioned and used in the circuit model are given in Table 1. Ref. 10 uses the electrode configuration detailed in Fig. 8.

Fig. 9 illustrates an approximation of the applied voltage square wave that was introduced in the experimental work of Roupassov et. al.[10] The slope that is introduced is to simulate a function that is differentiable. This is needed for $V'_{app}(t)$ in the governing differential equation as detailed by Eqs. 4-5. One could also generate a continuous function using Fourier decomposition of a traditional square wave, however this would not account for the minor rise and fall times found in experimentation.

B. 'Hot Spot' Results

For the small region of 0.4 mm x 0.4 mm over all time outside of the anode sheath, the time variation in the number density can be established. As an initial condition for Eq. 28, 10^{15} m^{-3} electrons were assumed

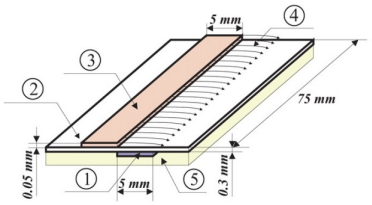

Figure 8. Experimental scheme used by Roupassov et. al[10] for the discharge gap. 1 high-voltage electrode; 2 dielectric layer; 3 low-voltage electrode, 4 zone of discharge propagation, 5 insulating plane.

Table 1. Experimental Parameters[11]

h_a	0.4 mm
h_d	0.3 mm
ϵ_d	2.7
ϵ_a	1
A_n	30 mm^2
A_d	30 mm^2
V	50 kV
ΔT	65 ns

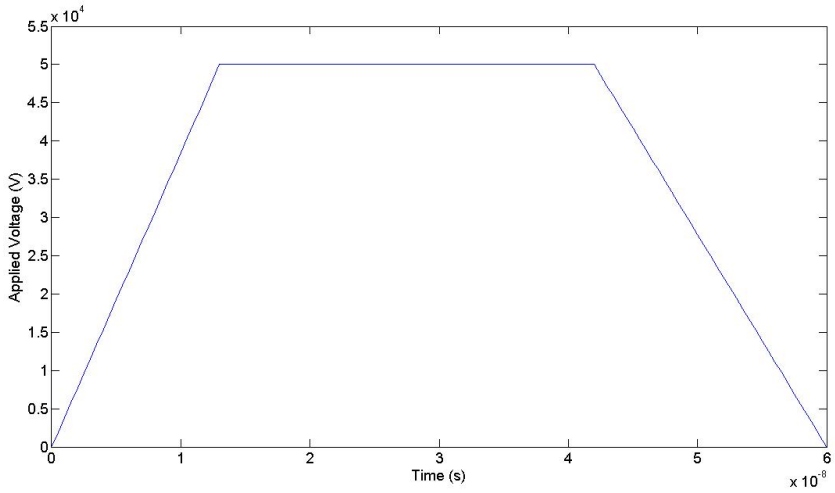

Figure 9. Plot of the input Voltage, V_{app} vs. time used in the model.

based on work by Ref. 10. As displayed in Fig. 10, there is a large gradient that occurs during the rise time that peaks around 1.13×10^{19} m^{-3}. It is also evident in Fig. 10 that the recombination of electrons is largely negligible on the nanosecond time scale. If a frequency of 1 kHz is used, the recombination of electrons with atoms allows a steady-state electron number density to be achieved on the nanosecond time scale. The recombination of electrons becomes a significant quantity when exploring the dynamics of a plasma discharge on the microsecond time scale.

Using Eq. 4 and Fig. 5, the model was able to produce a time-varying electron temperature. As displayed in Fig 11, there is an initial spike in the electron temperature to 29 eV (340 000 K) that coincides with the peak in electron number density at 11 ns. Fig. 11 also suggests that the assumption of a constant electron temperature is not an accurate assumption for nanosecond pulsed DBD plasmas. The variability

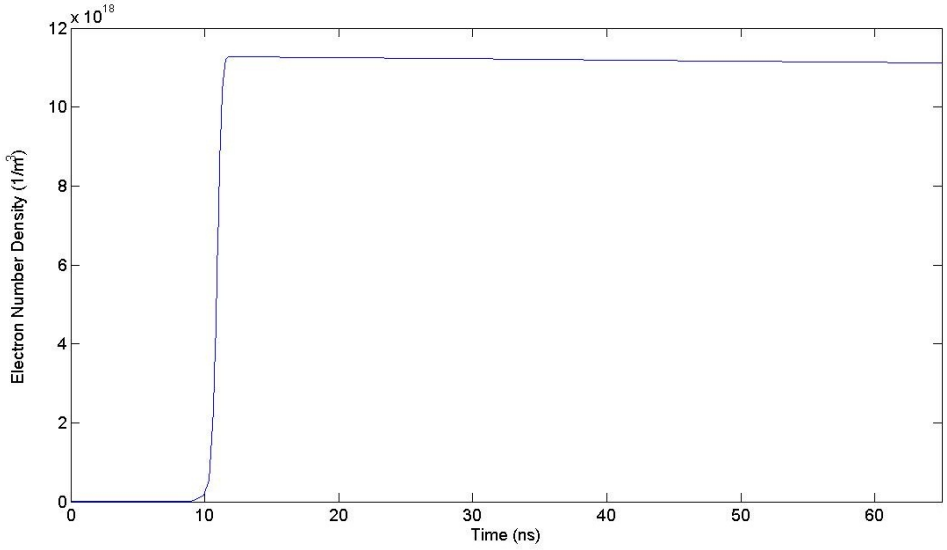

Figure 10. Plot of electron number density vs. time for the 'hot spot'.

in the electron temperature beyond 40 ns is due to the numerical error tolerances that are selected when solving Eqs. 4, 19 and 28. Fig. 11 shows that when reducing the relative error in the Dormand-Prince method from 10^{-2} to 10^{-3}, the strong functional variability experiences a significant reduction. The higher the gradients are during the rise and fall time, the finer the relative error tolerances are required to be to guarantee convergence of a solution.

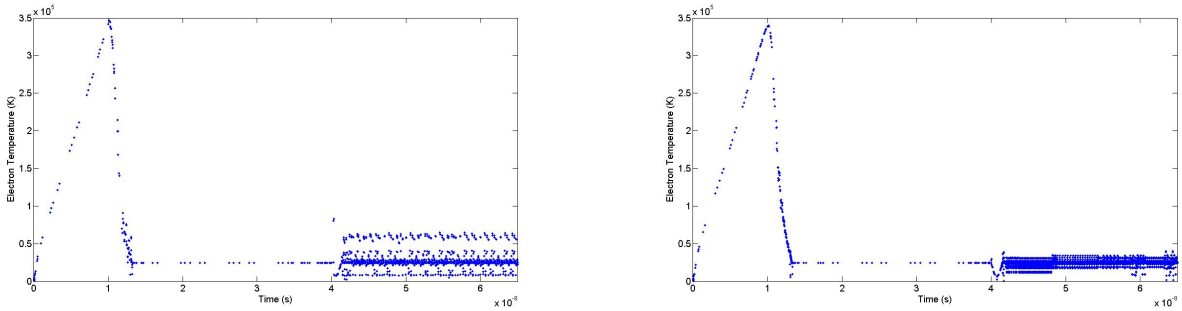

Figure 11. Plot of electron temperature vs. time for the 'hot spot'. Left- 10^{-2} error. Right- 10^{-3} error.

Using the results displayed in Figs. 10-11, the total power dissipated to neutral species as a function of time can be established. Using the result of Eq. 4 and the relationship for the instantaneous power, the time-varying power imparted to the flow can be given as[5]

$$P(t) = \frac{\Delta V^2(t)}{R_f(t)}. \tag{61}$$

As shown in Fig. 12, the instantaneous power is dominate during the rise time for the 'hot spot' region. Upon integrating the instantaneous power over time using Eq. 60, this model produces an energy value of 2.1 mJ for this region. When compared to the experimentally determined value of 4.2 mJ by Roupassov et. al,[10] this model produces an order of magnitude estimate for the energy imparted to neutral species in this region.

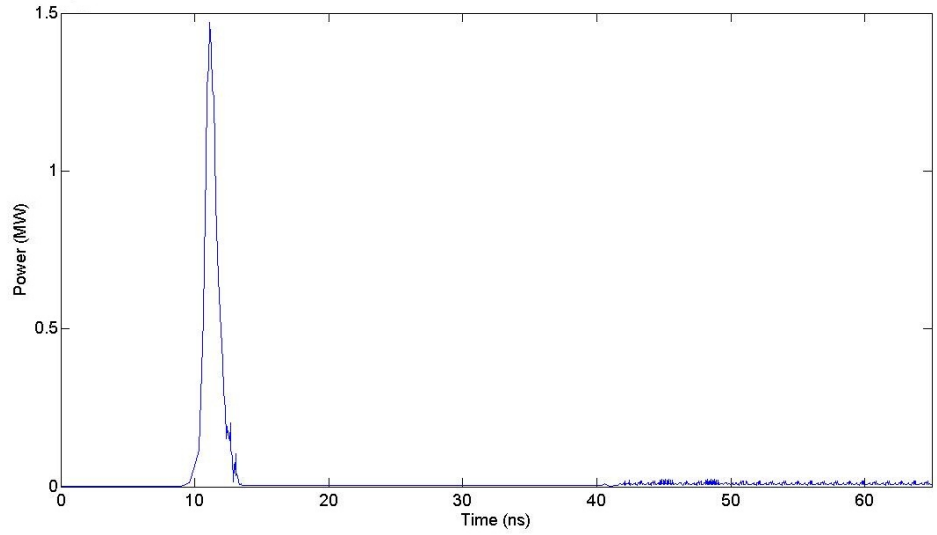

Figure 12. Plot of power vs. time for the 'hot spot'.

C. 'Hot Spot' Sheath Results

Using the Debye length approximation provided by Eq. 50 and the solution from the quasineutral 'hot spot' region ($n_e \sim 10^{19}$ 1/m^3, $T_e \sim 10$ eV) a Debye length of 7.43 μm is generated. The electron number density experienced in the anode sheath is assumed to be equal to the values calculated in the adjacent 'hot spot' region. Fig. 13 shows the time variation in the electron number density within the sheath and also shows a peak number density of 1.13×10^{19} m^{-3}.

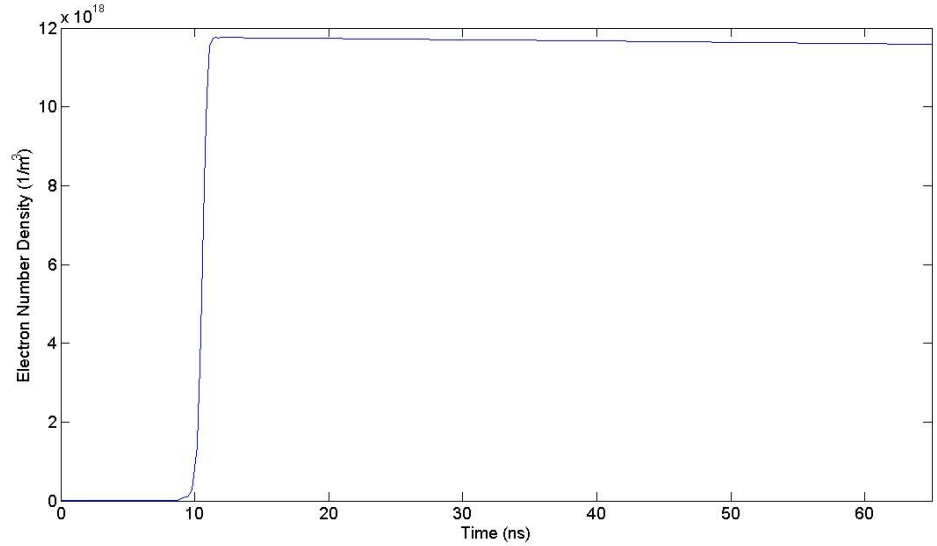

Figure 13. Plot of electron number density vs. time for the 'hot spot' sheath.

Using the revised form of the electric potential within the anode sheath given by Eq. 48 and using Fig. 5, the electric temperature variation over the duration of the pulse can be established. As displayed in Fig 14, there is an initial spike in the electron temperature to (348 000 K) that coincides with the peak in electron number density at 11 ns much like the hot spot region.

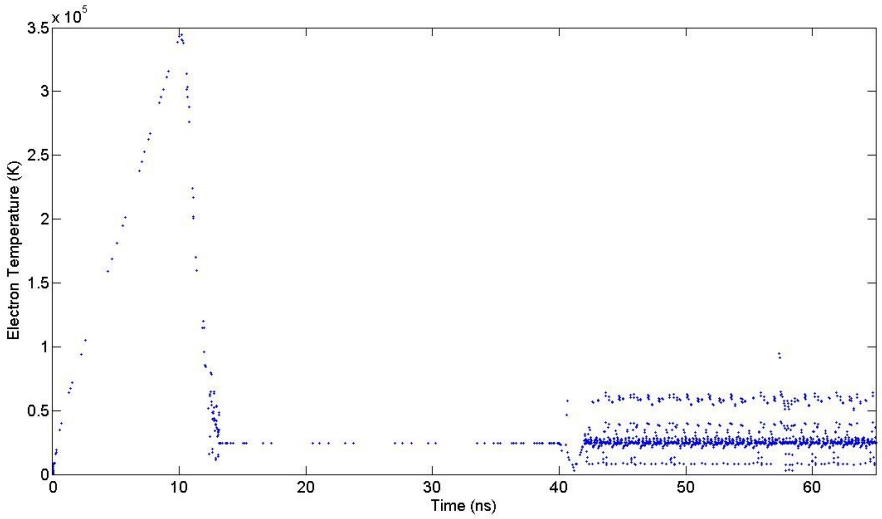

Figure 14. Plot of electron temperature vs. time for the 'hot spot' sheath.

As shown in Fig. 15, the instantaneous power is dominate during the rise time for the anode sheath region. Upon integrating the instantaneous power over time using Eq. 60, this model produces an energy value of 0.045 mJ for this region. This number is quite small compared to the 2.1 mJ experienced in the 'hot spot' region. However, the anode sheath does have a slightly higher linear energy density than the 'hot spot' region (6 J/m vs. 5.25 J/m). The reason that there is not significant deviation predicted in the anode sheath and quasineutral 'hot spot' regions is that explicit charge buildup is not accounted for in the circuit model within the sheath region. As shown by Ref. 13, the electric field in the sheath and adjacent quasineutral regions are approximately equal until charge buildup is allowed within the anode sheath during the length of the pulse or a series of pulses.

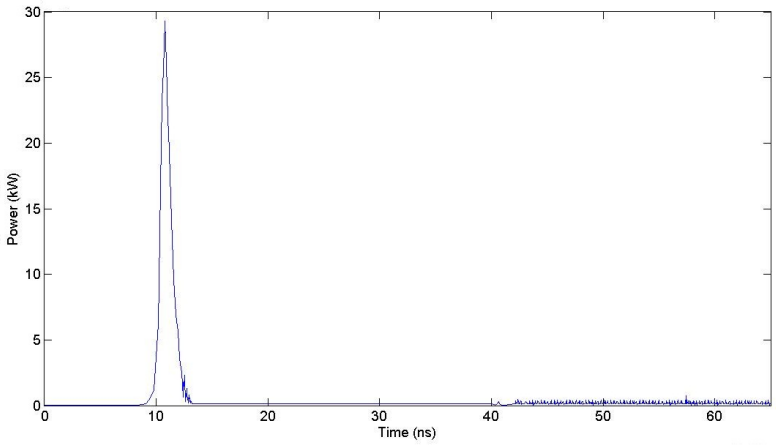

Figure 15. Plot of power vs. time for the 'hot spot' sheath.

D. 'Tail' Results

For the region 0.4 mm x 4.6 mm, the time variation in the number density can be established. As an initial condition for Eq. 28, 10^{15} m^{-3} electrons were assumed, the same number of electrons assumed for the 'hot spot' region. When comparing Figs. 10 and 16, the tail region experiences a lower growth rate in the number of electrons which is due to the lower electric field experienced by this region. As described by Eq. 28, a

lower electric field produces a lower number of ionizations and therefore a more gradual rise and lower total peak in N_e, approximately 3.4×10^{17}.

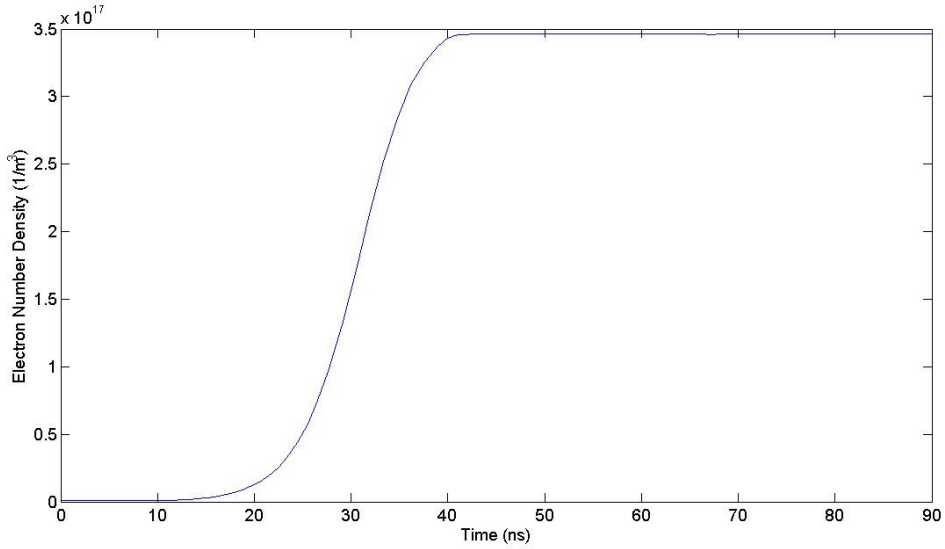

Figure 16. Plot of electron number density vs. time for the 'tail'.

Using Eq. 4 and Fig. 5 the model was able to produce a time-varying electron temperature. As displayed in Fig 17, the traditional assumption of 1 eV (11 600 K) does not agree well with the results obtained in this model for the tail region on the nanosecond time scale. Instead Fig. 17 suggests that the peak electron temperature is achieved during the rise time of the pulse, 220 000 K (19 eV) and then trends downward during the plateau portion of the voltage waveform. Much like Fig. 11, the highest electron temperatures are achieved during the initial high gradient of the pulse. Fig 17., unlike Fig. 11, also shows a rise in electron temperature during the fall time of the pulse as well. This is due to the lower electric potential and negative gradient experienced in the tail region during the fall time.

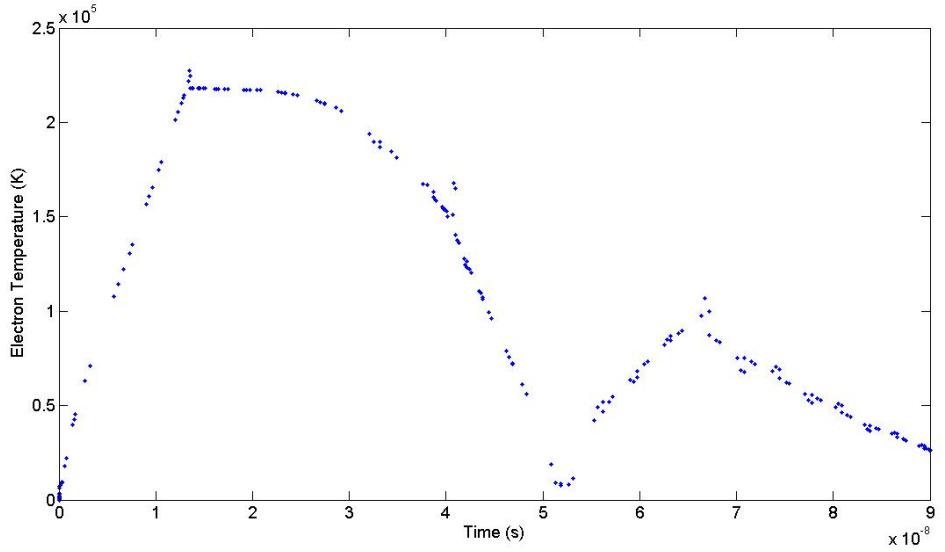

Figure 17. Plot of electron temperature vs. time for the 'tail'.

As shown in Fig. 18, the instantaneous power is dominate during the plateau portion of the applied voltage pulse for the 'tail' region. Upon integrating the instantaneous power over time using Eq. 60, this model produces an energy value of 6.6 mJ. When compared to the experimentally determined value of 8 mJ by Roupassov et. al,[10] this model produces an absolute error of $\approx 17.5\%$. The significant improvement in accuracy for the tail region can likely be attributed to the larger distance from the cathode. This increase in distance improves the assumptions of quasineutrality and that the spatial diffusion of charged species is negligible. The region close to the cathode features complicated ion and electron buildup and as the relative distance from the cathode increases, its impact on the problem becomes negligible.

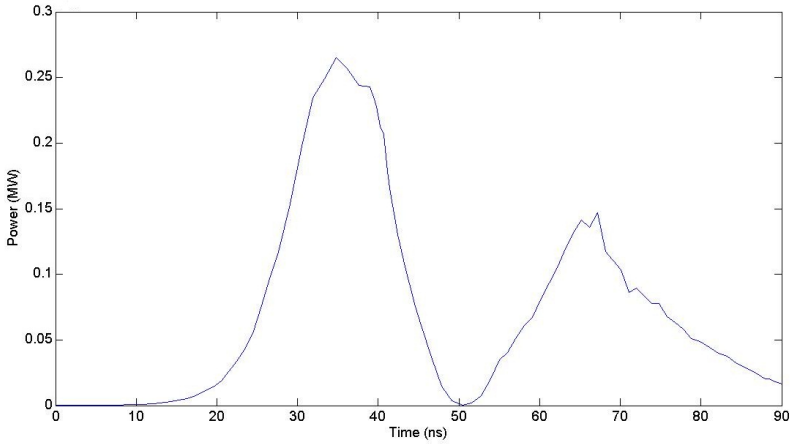

Figure 18. Plot of power vs. time for the 'tail'.

Table 2 summarizes the results obtained using the circuit model presented in this paper and associated experimental measurements made by Roupassov et. al[10] for both the 'hot spot' and 'tail' regions.

Table 2. Comparison between calculated and experimentally measured energy deposition.

	Circuit Model [mJ]	Experimental[10] [mJ]	Abs. Error [%]
'Hot Spot'	2.1	4.2	50.0
'Tail'	6.6	8.0	17.5
Total	8.7	12.2	28.7

IV. Conclusion

A new lumped element circuit model was presented that is valid for pulsed DC Dielectric Barrier Discharge (DBD) plasmas. The model approximates the total energy dissipated into neutral species using a lumped element circuit while containing relevant plasma physics in the form of a variable electron temperature and number density. An approximate expression was formulated using the conductivity of the discharge to calculate the resistance value for the air gap. Asymmetric wall effects were also approximated in the model by including the effect of the anode sheath. Results of the model were verified against a pulsed DC experiment conducted by Roupassov et. al[10] and order of magnitude agreement was obtained for the energy imparted into the plasma in both the homogeneous 'hot spot' region and 'tail' region.

Appendix

The momentum cross sections used for the numerical approximations in the model are shown in Table 3. These values were obtained by A.V. Phelps.[8]

Table 3. Momentum Cross Sections[8]

Kinetic Energy (eV)	N_2 (1E-16 cm^2)	O_2 (1E-16 cm^2)
1	10	7.2
2.1	27	6.6
3	21.7	5.7
4	12.6	5.5
5	10.9	5.6
10	10.4	5
15	11	8.8
20	10.2	8.6

References

[1]BOLSIG+ 2005 CPAT: http://www.codiciel.fr/plateforme/plasma/bolsig/bolsig.php

[2]Collins, George, W. Fundamental Numerical Methods and Data Analysis. Harvard Library. Web. http://ads.harvard.edu/books/1990fnmd.book/.

[3]C. L. Enloe, T. E. McLaughlin, R. D. VanDyken, K. D. Kachner, E. J. Jumper, T. C. Corke, M. Post, and O. Haddad, "Mechanisms and response of a single dielectric barrier plasma actuator: Geometric effects," AIAA Journal, 42(3):595604, 2004.

[4]Griffiths, David J. *Introduction to Electrodynamics*, Upper Saddle River, NJ: Prentice Hall, 1999.

[5]Orlov, D., Corke, T. and M. Patel, "Electric circuit model for aerodynamic plasma actuator," AIAA Paper 2006-1206, 2006.

[6]Orlov, D., "Modelling and Simulation of Single Dielectric Barrier Discharge Plasma Actuators," Ph. D. Dissertation, University of Notre Dame, 2006.

[7]Mitchner, M., Kruger, C.H. *Partially Ionized Gases*, John Wiley & Sons, Inc., Indianapolis, IN, 1973.

[8]Phelps A., http://jila.colorado.edu/ avp/collision_data/electronneutral/ELECTRON.TXT.

[9]Raizer, Yu P. *Gas Discharge Physics*, Springer, 1991. Chapter 4, Page 56.

[10]Roupassov, D.V., Nikipelov, A.A., Nudnova, M.M., and Starikovskii, A. Yu., "Flow separation control by plasma actuator with nanosecond pulse periodic discharge," *Gas Discharges and Their Applications*, 17th International Conference, pp.609-612, 7-12 Sept. 2008.

[11]Smirnov, B. M. *Physics of Ionized Gases*, Wiley, New York, 2001.

[12]Takashima, Keisuke, Yvette Zuzeek, and Walter R. Lempert. "Characterization of Surface Dielectric Barrier Discharge Plasma Sustained by Repetitive Nanosecond Pulses." AIAA Paper 2010-4764, 2010.

[13]Uddi, M., Jiang, N, and I. V. Adamovich, and W. R. Lempert, J. Phys. D 42, 075205, 2009.